RSC Advances

PAPER

View Article Online
View Journal | View Issue

Cite this: *RSC Adv.*, 2017, **7**, 26952

Synthesis of three-dimensional ordered mesoporous MnO_x/CeO_2 bimetal oxides for the catalytic combustion of chlorobenzene

Liyao Wu,[a] Fei He,[a] Jiaqi Luo[a] and Shantang Liu *[ab]

A series of CeO_2 supported ordered mesoporous MnO_x/CeO_2 bimetal oxides with 3-D bi-continuous pore structure were prepared by an incipient-wetness impregnation method, and used in the catalytic combustion of chlorobenzene (CB) as a model of dioxins. The as-synthesized catalysts were characterized by transmission electron microscopy (TEM), X-ray diffraction (XRD), hydrogen temperature-programmed reduction (H_2-TPR), X-ray photoelectron spectroscopy (XPS) and Brunauer–Emmett–Teller (BET) N_2 adsorption, respectively. The effect of pore structure and Mn loading content on catalytic properties and textural structure had been explored. On Mn/Ce(0.43) (molar ratio Mn/Ce equal to 0.43), the T_{90} (temperature at which 90% conversion is attained) is 279 °C. Compared with other MnO_x/CeO_2 samples with different Mn loading contents, the high activity of Mn/Ce(0.43) is ascribed to well dispersed MnO_x and a large amount of active chemisorbed oxygen species. This Mn/Ce(0.43) catalyst can maintain 90% CB conversion at 350 °C for at least 1000 min. And kinetics of on Mn/Ce(0.43) at 200 and 300 °C showed a dependence of rate on CB concentration is of first order, well within the inlet CB concentration from 500 to 2000 ppm. In addition, the T_{90} of Mn/Ce(0.43) is significantly lower than that of the general Mn/Ce-NPs, and the enhanced activity of Mn/Ce(0.43) is due to its bi-continuous 3-D ordered pore structure.

Received 24th February 2017
Accepted 14th May 2017

DOI: 10.1039/c7ra02299a

rsc.li/rsc-advances

1. Introduction

The emission of volatile organic compounds (VOCs) from a wide range of industrial processes or the incineration of municipal and medical waste,[1] contributing most to air pollution, continues to attract considerable public concern. Among these compounds, CVOCs (chlorinated volatile organic compounds), especially polychlorinated dibenzo-dioxins and dibenzo-furans (PCDDs and PCDFs, also named dioxins), have attracted the most public concern because of their persistence in the environment, bioaccumulation in tissues and potential toxicity as carcinogens and teratogens.[1] In many countries, stringent environmental regulations are established to limit PCDD/F emission.[2] Therefore, many technologies have been studied towards the elimination of CVOCs; catalytic combustion is one of the most effective and promising technologies for the destruction of CVOCs, with no production of secondary pollutants, low energy consumption and even very dilute pollutants can be treated efficiently without additional fuel compared with conventional thermal processes. Considering PCDD/Fs' high toxicity, we use chlorobenzene (CB) as the model compound to evaluate the catalytic behaviors on the catalysts, because of its structural similarity to dioxins.

To date, catalysts that have been investigated for catalytic combustion of chlorobenzene, can be divided mainly into three broad categories, namely noble metals,[3,4] metal oxides[5–7] and zeolites.[8,9] The activities of zeolites are related to their acid properties, special three-dimensional channel structure, high internal surface area and good thermal stability.[10] Though noble metal catalysts express considerable catalytic activity, they are susceptible to the deactivation by chlorine poisoning,[11] and easily produce undesirable polychlorinated biphenyls byproducts, let alone the high cost. Metal oxides are also active for catalytic removal of CVOCs and they are environmentally benign and economically viable, which are gaining increasing attention. For example, Wang *et al.*[12] prepared MnO_x–CeO_2 mixed oxide catalysts which exhibited excellent catalytic performance for CB degradation, the complete combustion temperature was 279 °C, an inspiring discover and powerful evidence of Mn–Ce bimetal oxides for practical application.

As we know, cerium dioxide is known to be an excellent support or promoter in various catalytic processes due to its unique oxygen storage capability and oxygen transfer ability,[13–15] and the oxygen storage capability as well as the catalytic property of ceria is intimately associated with the shape of the particles.[16] For example, CeO_2 nanorods are remarkably more

[a]*Key Laboratory for Green Chemical Process of Ministry of Education, School of Chemistry and Environmental Engineering, Wuhan Institute of Technology, Wuhan 430074, PR China. E-mail: stliu@wit.edu.cn; Tel: +86 27 87195001*

[b]*Wuhan Industrial Institute for Chemical Advanced Material Limited Liability Company, Wuhan 430074, PR China*

active for CO oxidation than the traditional spherical nanoparticles.[17,18] In 2011, Wu *et al.*[19] synthesized 3D-like CeO_2 microflowers and microspheres, revealed that 3D-like ceria show great superiority for formation of oxygen vacancies, which in turn leads to higher oxygen mobility and reducibility. Pure CeO_2 is susceptible to Cl poisoning,[20] hence other metal components were often introduced to form polymetallic oxides for improving the resistance to Cl poisoning. In the past two decades, Mn–Ce bimetal oxides have been widely explored as catalysts for the abatement of various pollutants,[21–26] such as CO oxidation, selective catalytic reduction of NO_x with NH_3, and oxidation of volatile organic compounds, because of their remarkable catalytic properties. In 2014, we[27] have investigated the effect of CeO_2 morphology on the performance of MnO_x/CeO_2 catalysts for the catalytic combustion of chlorobenzene (CB), and found that CeO_2 morphology has an important influence on the exposure extent of different lattice plane, which is crucial to the catalytic performances. In 2013, Cui *et al.*[28] studied the effect of preparation method on MnO_x–CeO_2 catalysts for NO oxidation.

Additional studies revealed that MnO_x/CeO_2 catalysts exhibited excellent catalytic performance in the combustion of CB. However, in previous researches, most attention was concentrated on the morphology effect and novel synthesis methods, little attention has been attached to the effect of porous-framework structure of MnO_x/CeO_2 bimetal oxides for catalytic combustion of CB catalytic combustion of chlorobenzene is a typical heterogeneous catalytic reaction. For heterogeneous catalytic reaction, to the best of our knowledge, the activity of catalyst is closely linked to the pore structure, different pore structure can affect the mass transfer process, hence influencing catalytic efficiency. Herein, we developed novel CeO_2 supported MnO_x/CeO_2 bimetal oxides with 3-D bicontinuous mesoporous structure *via* incipient-wetness impregnation method for elimination of CB, CeO_2 support was prepared *via* nanocasting method by using ordered mesoporous silica (KIT-6) as the template. This nanocasting method is also suitable for synthesis of other metal oxides with 3-D ordered porous structure. For comparison, pure MnO_x and MnO_x/CeO_2 nanoparticles were also prepared, which have no internal porous structure. The effect of pore structure and Mn loading content on catalytic properties here had been explored.

2. Experimental sections

2.1. Catalysts preparation

2.1.1. Preparation of KIT-6 template. Ordered mesoporous silica (KIT-6) with *Ia3d* symmetry was used as a hard template and was synthesized according to a previous report.[29] Briefly, 6 g Pluronic 123 ($EO_{20}PO_{70}EO_{20}$) was dissolved in a solution of 11.8 g concentrated HCl (35%) and 217 g ultrapure water. To this, 6 g *n*-butanol was added under stirring at 35 °C. After vigorous stirring for 1 h, 12.9 g tetraethyl orthosilicate (TEOS) was added to the solution, which was then stirred for 24 h at this temperature. Subsequently the milky suspension was transferred to a Teflon-lined stainless steel autoclave and placed in an oven at 100 °C for 24 h. The white solid product was filtered, dried at 80 °C overnight, and finally calcined in air at 550 °C for 5 h.

2.1.2. Preparation of ordered mesoporous MnO_x/CeO_2 catalysts. The ceria support was synthesized by nanocasting method using KIT-6 as the template and cerium nitrate hydrate ($Ce(NO_3)_3 \cdot 6H_2O$) as cerium source, followed by removal of the silica template using 2 M NaOH solution. In a typical synthesis, 4.37 g $Ce(NO_3)_3 \cdot 6H_2O$ was dissolved in 20 ml anhydrous ethanol, and 0.5 g KIT-6 was added into this homogenous solution under vigorous stirring. The mixture was stirred for 3 h at room temperature, and then the ethanol was evaporated at 60 °C. The obtained dry powder was heated to 300 °C at a rate ratio of 2 °C min^{-1} and calcined at this temperature for 5 h. The impregnation procedure was then repeated with half the amount of cerium nitrate hydrate, and the final impregnation product was calcined at 550 °C for 5 h. The resulting sample was treated with 2 M NaOH solution to remove the silica template, centrifuged, washed several times with water and dried at 80 °C in air. This template-free CeO_2 was denoted as replica CeO_2. For comparison, we obtained CeO_2 nanoparticles (denoted as CeO_2-NPs) by directly calcining $Ce(NO_3)_3 \cdot 6H_2O$ at 400 °C for 4 h. And pure MnO_x was obtained by calcining $Mn(NO_3)_2 \cdot 4H_2O$ (97 wt%) at 400 °C for 4 h.

MnO_x/CeO_2 bimetal oxides were prepared by the incipient wetness impregnation method. In a typical process, a certain amount of $Mn(NO_3)_2$ (50 wt%) was dissolved in ultrapure water, and the solution was added to replica CeO_2. Following impregnation, they have to rest at room temperature for 48 h, and then dried at 80 °C overnight, finally calcined in air at 400 °C for 4 h. For studying the effect of Mn loading content, here we synthesized several samples with different Mn/Ce molar ratios, in the range from 0.11 to 0.67, named as Mn/Ce(0.11), Mn/Ce(0.25), Mn/Ce(0.43), Mn/Ce(0.67), respectively. For comparison, using CeO_2-NPs as support, we prepared MnO_x/CeO_2 nanoparticles (denoted as Mn/Ce-NPs) with Mn/Ce molar ratio equal to 0.43.

2.2. Catalysts characterization

The phase structures of prepared catalysts were analyzed by X-ray diffraction (XRD) using an X-ray diffractometer (Rigaku MiniFlex600) with Cu Karadiation (40 kV and 40 mA). Nitrogen adsorption and desorption isotherms were measured on a Micromeritics ASAP2460 nitrogen-adsorption apparatus. The specific surface areas of samples were measured using the Brunauer–Emmett–Teller (BET) method, and the pore volumes and pore size distributions were determined using the Barrett–Joyner–Halenda (BJH) method. Transmission electron microscopy (TEM) images were acquired using a JEOL JEM-2100 microscope. The samples were ground up using a mortar, suspended in ethanol and mounted onto Cu grids. The surface atomic states of the catalysts were analyzed by X-ray photoelectron spectroscopy (Thermo Scientific K-Alpha XPS). The temperature-programmed reduction (TPR, Micro 2920) runs were conducted with a linear heating rate (10 °C min^{-1}) in a flow of 10% H_2 in argon at a flow rate of 40 ml min^{-1}.

2.3. Catalytic activity measurements

Catalytic activity tests were performed in a quartz tube micro-reactor with an 8 mm inner diameter under an atmospheric pressure. 0.2 g catalysts were placed in the center of the reactor. The feed gases were consisted of 1000 ppm CB, 20% O_2, and balanced N_2, the total flow rate was 100 ml min^{-1} and gas hourly space velocity (GHSV) at 15 000 h^{-1}. Catalytic performance tests were performed at temperature range of 100–400 °C, and the tests of all catalyst were stabilized for at least 20 min at each temperature for each CB concentration. The effluents were analyzed by an on-line gas chromatograph (GC) equipped with a flame ionization detector (FID) for the quantitative analysis of CB.

3. Results and discussions

3.1. Catalytic performance results

The performance results for catalytic combustion of CB over the as-synthesised catalysts are shown in Fig. 1. For pure replica CeO_2, the conversion reaches 25% at 200 °C, then it begins to deactivate, the conversion drops to 1% at 300 °C, due to strong adsorption of HCl and Cl on CeO_2 surface.[30] With further increasing reaction temperature, the conversion of CB gradually increases again. The activity and stability is obviously improved after the incorporation of MnO_x into CeO_2. The activity increases with increasing Mn/Ce molar ratio from 0.11 to 0.67, and Mn/Ce(0.43) shows the highest efficiency, T_{50} and T_{90} (the temperature needed for the conversion of 50% and 90%, respectively) are 199 °C and 279 °C, respectively. T_{90} of Mn/Ce(0.67) is 310 °C, the activity is little worse than Mn/Ce(0.43). In addition, Mn/Ce-NPs almost show no reaction activity under 200 °C. The activity of Mn/Ce(0.43) is significantly higher than Mn/Ce-NPs. For pure MnO_x, T_{90} is 339 °C, a fairly low activity than Mn/Ce(0.43).

3.2. Catalyst characterization

3.2.1. XRD. Low-angle XRD patterns of replica CeO_2 and MnO_x/CeO_2 are displayed in Fig. 2. For replica CeO_2, there is a well-resolved peak at $2\theta = 0.86°$ corresponding to a cubic *Ia3d* symmetry with d_{211} spacing,[31] demonstrating well-ordered pore arrangement. After Mn doping, the diffraction peaks do not shift and retain intense peaks at 0.86°, illustrating all samples possess well ordered structures.

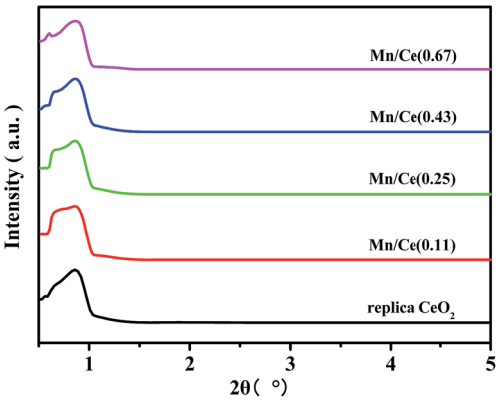

Fig. 2 Low-anger XRD patterns of the as-synthesized samples.

Wide angle XRD patterns of MnO_x/CeO_2 bimetal oxide catalysts with various Mn/Ce molar ratios are shown in Fig. 3. For replica CeO_2, the diffraction peaks at 2θ = 28.6°, 33.1°, 47.5°, 56.3°, 59.1°, 69.4° are indexed well to a typical cerium cubic fluorite-like structure (JCPDS 43-1002). After loading Mn, all the MnO_x/CeO_2 catalysts still maintain cerium cubic fluorite structures, no peaks of manganese oxides are observed, which may be ascribed to well dispersion of MnO_x on CeO_2 surface or formation of very small MnO_x nanoparticles. As Mn loading content increases, the intensity of the diffraction peaks decrease gradually, which represent weakening crystallinity degree of the samples. Additionally, the general Mn/Ce-NPs also show cerium cubic fluorite structures.

3.2.2. TEM. Fig. 4 displays the TEM images of replica CeO_2 and MnO_x/CeO_2 bimetal oxide catalysts. TEM was performed to analyze the mesoporous structure of the samples and dispersion of Mn species on support. From the TEM images, we can clearly see that replica CeO_2 exhibit well-order cubic array structures. With increasing Mn loading content, Mn/Ce(0.11) and Mn/Ce(0.43) still maintain well-ordered mesoporous

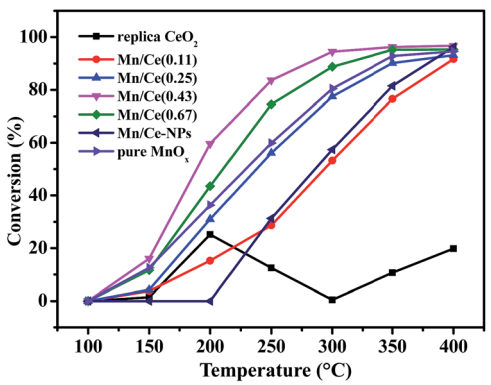

Fig. 1 Replica CeO_2, pure MnO_x and MnO_x/CeO_2 catalysts for CB combustion, gas composition: 1000 ppm CB, 20% O_2, N_2 balance; GHSV = 15 000 h^{-1}.

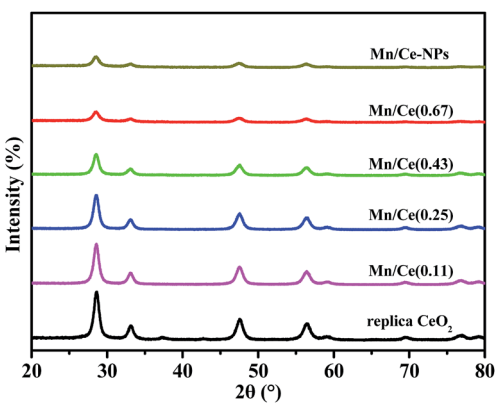

Fig. 3 Wide-anger XRD patterns of the as-synthesized samples.

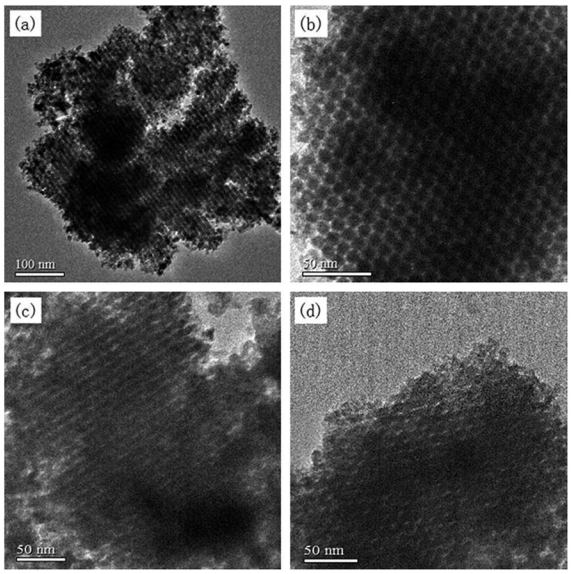

Fig. 4 TEM images of the samples: (a) replica CeO_2; (b) Mn/Ce(0.11); (c) Mn/Ce(0.43); (d) Mn/Ce(0.67).

structures, and no obvious aggregation is observed. But for Mn/Ce(0.67), it generally maintained ordered mesoporous structure, the aggregation of MnO_x on CeO_2 surface can be clearly observed, which likely causes the reduction of the reducibility. In addition, we can detect that the pore diameters decrease slightly with increasing Mn loading content, ascribing to incorporation of more MnO_x into internal channels of CeO_2, which accordingly causes the decrease of pore volume and special surface area (Table 1), thus slowing down the mass transfer process.

3.2.3. BET. To examine the pore sizes and their distributions, nitrogen adsorption–desorption measurement was carried out (Fig. 5). For all samples, typical IV isotherms with H_2-type hysteresis loop can be observed in Fig. 5A.[32,33] The pore size distributions, calculated from the N_2 desorption isotherms, are shown in Fig. 5B. And it shows that all samples exhibit bimodal pore size distributions. For replica CeO_2, the smaller pore size is centered at about 3.2 nm, the large one is centered at about 10.55 nm. The same results have been reported by Wen *et al.*,[34,35] namely the nanocast metal oxides show a bimodal pore size distribution. Of course, the main pore size is the large ones for all samples. And the relevant textural properties obtained from the nitrogen sorption isotherm are summarized in Table 1. We could see the specific surface area, pore diameter

Table 1 Properties of MnO_x/CeO_2 catalysts

Samples	Surface area ($m^2\ g^{-1}$)	Pore size (nm)	Pore volume ($cm^3\ g^{-1}$)
Replica CeO_2	69.96	10.55	0.16
Mn/Ce(0.11)	62.47	10.37	0.15
Mn/Ce(0.43)	46.01	10.03	0.10
Mn/Ce(0.67)	44.50	9.87	0.10

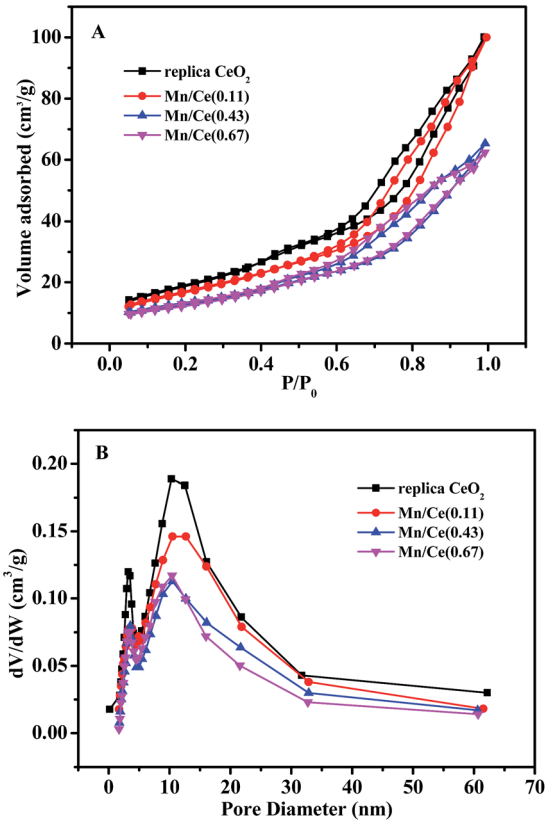

Fig. 5 (A) N_2 adsorption–desorption isotherms and (B) pore-size distributions of the samples.

and the pore volume of replica CeO_2 are 70.0 $m^2\ g^{-1}$, 10.0 nm, 0.17 $cm^3\ g^{-1}$, respectively. With increasing Mn content, the pore sizes hardly change, but the specific surface area and pore volume decrease, due to more Mn species entering into 3-D channels of CeO_2.

3.2.4. H_2-TPR. The redox properties of replica CeO_2 and MnO_x/CeO_2 bimetal oxides were examined by H_2-TPR analysis, and the H_2-TPR profiles of the as-synthesized catalysts are shown in Fig. 6. In the TPR curve of replica CeO_2, the reduction peaks occur at 432 °C with a shoulder peak at 505 °C, assigned

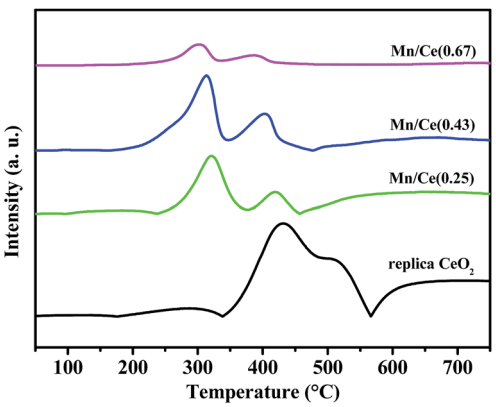

Fig. 6 H_2-TPR profiles of the as-synthesized samples.

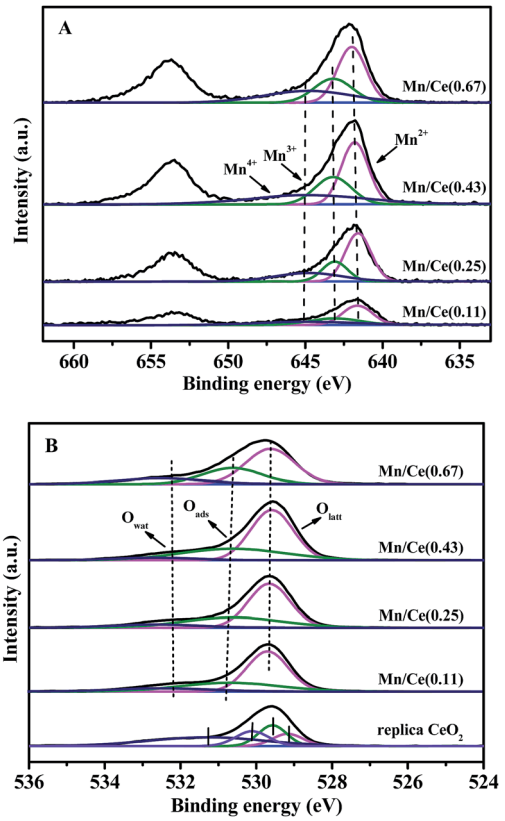

Fig. 7 (A) Mn $2p_{3/2}$ spectras and (B) O 1s spectras of the samples.

to the reduction of surface capping oxygen of CeO_2.[36] With doping Mn into CeO_2, for all MnO_x/CeO_2 catalysts, two peaks are observed, the former is related to the reduction of MnO_2/Mn_2O_3 to Mn_3O_4, the later is related to the reduction of Mn_3O_4 to MnO.[37] After loading Mn, the reduction temperatures of all MnO_x/CeO_2 bimetal oxides systematically shift to low values. For Mn/Ce(0.25), the two reduction peaks are at about 321 and 419 °C, respectively. In the TPR profiles of Mn/Ce(0.43), two broad reduction peaks at about 313 °C and 403 °C can be observed, the temperatures shift to low values for comparison with Mn/Ce(0.25), indicating that Mn/Ce(0.43) has stronger reducibility than Mn/Ce(0.25). For Mn/Ce(0.67), the two reduction peaks are at about 301 and 386 °C, respectively. Though Mn/Ce(0.67) exhibits good reducibility, the amount of H_2 consumption is much less than Mn/Ce(0.43), indicating that Mn/Ce(0.43) has more active oxygen species. And the activity of Mn/Ce(0.43) is higher than Mn/Ce(0.67) for catalytic combustion of CB, indicating that the active oxygen species play a crucial role in catalytic combustion of CB for comparison with the reducibility over the catalysts here.

3.2.5. XPS. The Mn $2p_{3/2}$ and O 1s XPS spectras of MnO_x/CeO_2 catalysts with different Mn loading contents are present in Fig. 7. Proportions of the surface compositions of the catalysts were estimated from the XPS results and are shown in Table 2. The Mn $2p_{3/2}$ spectrum of all samples can be deconvoluted into three distinguish peaks at 641.5–642.0 eV, 643.1–643.2 eV and 644.8 eV (binding energy), which can be ascribed to Mn^{2+}, Mn^{3+} and Mn^{4+}, respectively, confirming the coexistence of three kinds of Mn species.[38] Because no crystalline MnO, Mn_2O_3 or MnO_2 species were detected on all the catalysts by XRD, MnO, Mn_2O_3 or MnO_2 in the catalysts might be well dispersed on the catalyst surface in the amorphous state.[39] As shown in Table 2, the atom ratio of Mn^{4+} in surface compositions continues to increase from 1.8% to 3.3% as Mn loading ratio increases from 0.1 to 0.4. As reported in previous work, higher oxidation state of manganese species was found to be preferable for oxidation reactions over the manganese-containing catalysts,[40] and high valent Mn^{4+} can lead to oxygen vacant sites on catalysts, which is helpful for oxidation reactions.[41] The atom ratios of Mn^{4+} on Mn/Ce(0.43) surface is 3.2%, which has a small difference with Mn/Ce(0.67) of 3.3%.

O 1s spectrum of replica CeO_2 in Fig. 7B shows two peaks at 529.2, 529.6 eV, assigned to lattice oxygen.[42] Two shoulder peaks at 530.1 and 531.3 eV are observed, which can be attributed to adsorbed oxygen and weakly bonded oxygen species (active oxygen),[43] and to surface oxygen by hydroxyl species and adsorbed water species presser as contaminants at the surface, respectively.[44] The O 1s profile of MnO_x/CeO_2 catalysts can be fitted into three peaks: lattice oxygen (O_{latt}) at 529.6–529.7 eV, adsorbed oxygen (O_{ads}) at 530.6–530.7 eV, molecular water (O_{wat}) at 532.4–532.6 eV, respectively. In comparison with replica CeO_2, lattice oxygen of MnO_x/CeO_2 bimetal oxides slightly shift to higher values, because of "Mn ← O" electron-transfer process, indicating the existence of more abundant electrophilic group, namely active oxygen species (*e.g.*, O_2^-, $O_2^{=}$, O^-, $O^{\bullet}$) on catalysts' surface.[45] With the increase of molar ratio Mn/Ce from 0.11 to 0.67, the amount of adsorbed oxygen increases from 22.5% to 24.4%. O_{ads} is the most active oxygen species and higher concentration of O_{ads} is helpful for catalytic oxidation of CB due to its high mobility.[46] From Table 2, we can

Table 2 The XPS results of MnO_x/CeO_2 catalysts with various Mn contents

				Mn distribution (%)			O distribution (%)		
Catalysts	Mn (%)	Ce (%)	O (%)	Mn^{2+}	Mn^{3+}	Mn^{4+}	O_{latt}	O_{ads}	O_{wat}
Replica CeO_2	0.0	24.0	76.0	0.0	0.0	0.0	29.5	15.0	31.5
Mn/Ce(0.11)	4.8	22.4	72.8	2.3	0.7	1.8	41.8	22.5	8.5
Mn/Ce(0.25)	7.9	19.9	72.2	4.3	1.7	1.9	42.7	23.1	6.4
Mn/Ce(0.43)	10.6	18.0	71.4	4.7	2.7	3.2	42.8	24.4	4.2
Mn/Ce(0.67)	11.5	18.1	70.4	5.2	3.0	3.3	38.3	21.0	11.1

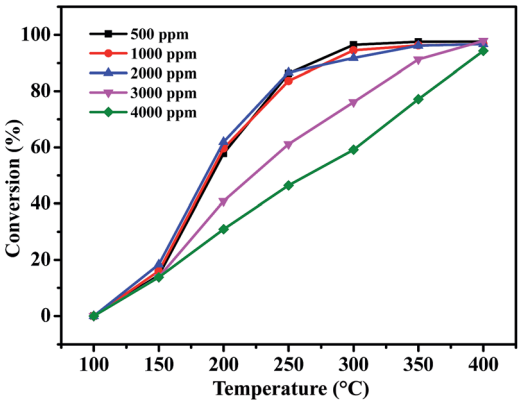

Fig. 8 The effect of CB concentrations on the activity of Mn/Ce(0.43) catalyst; gas composition: 500–4000 ppm of CB, 10% O_2, N_2 balance; GHSV = 15 000 h^{-1}.

see the amount of O_{latt} keeps growing with the increase of Mn content from 0.1 to 0.3, but for Mn/Ce(0.67), the O_{latt} content decreases, which may be caused by MnO_x aggregation on Mn/Ce(0.67) surface. Hence, it was found that the dispersion of surface MnO_x and the amount of active oxygen species are the main factors influencing the catalytic activity here, Mn/Ce(0.43) is the most efficient catalyst for catalytic combustion of CB.

3.2.6. Effect of inlet CB concentration on CB catalytic combustion. The effect of inlet CB concentration on the conversion of CB over Mn/Ce(0.43) catalyst at the space velocity of 15 000 h^{-1} was investigated. Fig. 8 shows the conversion curves for catalytic combustion of CB with inlet concentration from 500 to 4000 ppm.

From Fig. 8, we can see that when the inlet CB concentration is 500 ppm, the T_{90} is the lowest, and the conversion of CB has a mild variation with the inlet CB concentration from 500 to 2000 ppm. However, the CB conversion decreases obviously when the CB inlet concentration increases to 3000 ppm or 4000 ppm, which is related to the deactivation of Mn/Ce(0.43) catalyst in higher CB concentration. In conclusion, the Mn/Ce(0.43) catalyst here exhibits highly activity when the inlet CB concentration is less than 2000 ppm.

3.2.7. Kinetics consideration. The effect of inlet CB concentration on the reaction rate on Mn/Ce(0.43) was investigated when the reaction proceeded at the space velocity of 15 000 h^{-1} at 200 °C and 300 °C, respectively. The catalyst was stabilized for 20 min at each temperature for each CB concentration. Fig. 9 shows that reaction rate varies in different manners with the inlet CB concentration increasing from 500 to 4000 ppm. When the reaction rate is tested at 200 °C, dependence of rate on CB concentration is of first order within the range from 500 to 2000 ppm of CB. However, from 2000 up to 4000 ppm of CB concentration, the rate lines maintain flat, and the reaction can be described well by zero order kinetics, the observed zero-order kinetics suggests that the catalyst surface is saturated by the reacting species within the overall reaction time and CB adsorption on the surface of Mn/Ce(0.43) at 200 °C must not be rate limiting.[38] Therefore, the doping of Mn into CeO_2 not only remarkably improves the catalytic efficiency but also highly promotes the resistance to chlorine poisoning from CB. But with the extended reaction time, the conversion still decreases gradually. The reaction is probably limited by one of the processes on the surface that follows adsorption, *e.g.*, reaction with oxygen species and desorption of products, such as Cl species, which has an inhibition effect on the reaction.[47–49] When the reaction rate was tested at 300 °C, dependence of reaction rate on concentration is also of first order within the range from 500 to 2000 ppm of CB, but from 2000 up to 4000 ppm of CB concentration, the reaction rate slow down, probably due to the gradual deposition of more Cl species produced during the decomposition of CB.

3.2.8. Stability study. The deactivation of catalysts for catalytic combustion of CVOCs is still a puzzle in commercial applications. In previous catalytic combustion of CB tests, replica CeO_2 was found rapidly deactivated due to strong adsorption of Cl on active sites. Fig. 10 presents the experimental results of stability test of Mn/Ce(0.43) catalyst at 350 °C and every 60 min we recorded the conversions of CB. We find Mn/Ce(0.43) catalyst shows good stability, the conversion can maintain 90% at 350 °C for at least 1000 min. Therefore, the doping of Mn into CeO_2 not only remarkably improves the

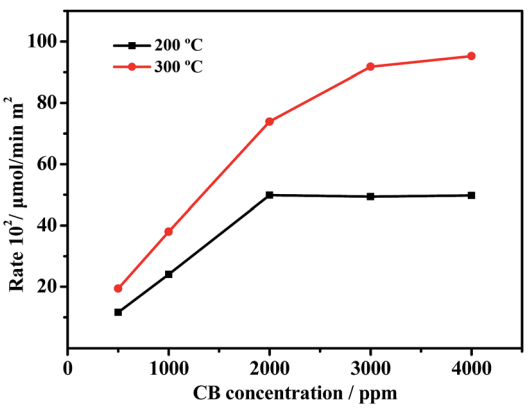

Fig. 9 The reaction rate at different CB concentrations over Mn/Ce(0.43) catalyst; gas composition: 1000 ppm CB, 20% O_2, balance N_2; GHSV = 15 000 h^{-1}.

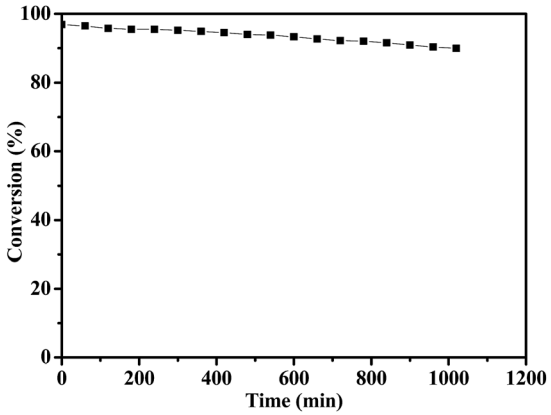

Fig. 10 The stability test over the Mn/Ce(0.43) catalyst for CB combustion at 350 °C; gas compositions: 1000 ppm of CB, 20% O_2, N_2 balance; GHSV = 15 000 h^{-1}.

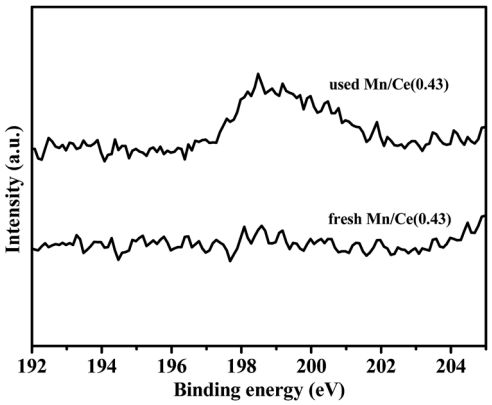

Fig. 11 Cl 2p spectras of fresh Mn/Ce(0.43) and used Mn/Ce(0.43).

catalytic efficiency but also highly promotes the resistance to chlorine poisoning from CB. But with the extended reaction time, the conversion still decreases gradually. The thermostability of cerium based catalysts here is still needed to be improved. And none intermediate products or byproducts have been detected by an on-line gas chromatograph (GC) equipped with a flame ionization detector (FID) during our stability test of Mn/Ce(0.43), this may be related to the detection limit of GC, but it fully demonstrates that the amount of byproducts is extremely trace. The selectivity to CO_2 here is nearly more than 99%, which is consistent with literature reports. In 2015, Yang *et al.*[50] also reported that all the 4Ce 1 M catalysts represented more than 99.5% selectivity to CO_x (more than 99% CO_2 and trace of CO) when all the organic compounds are completely destroyed and few byproducts dichlorobenzene-*m*, dichlorobenzene-*o* or dichlorobenzene-*p* were detected. And Wang *et al.*[51] reported that all the mixed oxide MnO_x–CeO_2 catalysts prepared by sol–gel method provided more than 99.5% selectivity to carbonoxides (more than 98% CO_2 and trace CO) and no polychlorinated benzene or other detectable C-containing byproducts were found.

The XPS spectras of Cl 2p of fresh and used Mn/Ce(0.43) are present in Fig. 11. It can be seen that the Cl species deposited on the surface of the used Mn/Ce(0.43), indicating that the deactivation of Mn/Ce(0.43) can be ascribed to strong adsorption of Cl species on catalyst surface that caused the blockage of active sites.

4. Conclusions

A series of ordered mesoporous MnO_x/CeO_2 bimetal oxides with Mn/Ce molar ratios in the range from 0.11 to 0.67 were successfully prepared and were examined for their performance on the catalytic oxidation of CB. Comparing with general Mn/Ce-NPs, Mn/Ce(0.43) performances better CB degradation ability, T_{90} is 101 °C lower than Mn/Ce-NPs. The highly improved activity is due to the special ordered 3-D channels, which facilitates the mass transfer process hence reducing the deposition of Cl species, despite of low specific surface area of this catalyst. Among the catalysts with different Mn supporting ratios, Mn/Ce(0.43) is the most efficient catalyst for catalytic combustion of CB, due to good MnO_x dispersion and large amount of active oxygen species.

Acknowledgements

We gratefully acknowledge the funding from the National Natural Science Foundation of China (No. 21603168, 21471120), Natural Science Foundation of Hubei Province (No. 2011CDA049), International Cooperation Foundation of Hubei Province (2012IHA00201), Educational Commission of Hubei Province of China (T201306).

Notes and references

1 A. A. Meharg and D. Osborn, *Nature*, 1995, **375**, 353–354.
2 S. Scirè and L. F. Liotta, *Appl. Catal., B*, 2012, **125**, 222–246.
3 S. Gil, J. M. Garcia-Vargas, L. F. Liotta, G. Pantaleo, M. Ousmane, L. Retailleau and A. Giroir-Fendler, *Catalysts*, 2014, **5**, 671–689.
4 R. W. van den Brink, R. Louw and P. Mulder, *Appl. Catal., B*, 1998, **16**, 219–226.
5 F. Bertinchamps, M. Treinen, P. Eloy, A. M. D. Santos, M. M. Mestdagh and E. M. Gaigneaux, *Appl. Catal., B*, 2007, **70**, 360–369.
6 J. Lichtenberger and M. D. Amiridis, *J. Catal.*, 2004, **223**, 296–308.
7 D. A. Aguilera, A. Perez, R. Molina and S. Moreno, *Appl. Catal., B*, 2011, **104**, 144–150.
8 M. Guillemot, J. Mijoin, S. Mignard and P. Magnoux, *Appl. Catal., A*, 2007, **327**, 211–217.
9 W. Zhao, J. Cheng, L. Wang, J. Chu, J. Qu, Y. Liu, S. Li, H. Zhang, J. Wang and Z. Hao, *Appl. Catal., B*, 2012, **127**, 246–254.
10 P. Yang, X. Xue, Z. Meng and R. Zhou, *Chem. Eng. J.*, 2013, **234**, 203–210.
11 J. V. De, M. K. Cieplik and R. Louw, *Environ. Sci. Technol.*, 2004, **38**, 5217–5223.
12 X. Wang, Q. Kang and D. Li, *Appl. Catal., B*, 2009, **86**, 166–175.
13 Y. Zheng, J. Wang, R. Zou, L. Liu, Z. Zhang and X. Wang, *Energy Fuels*, 2012, **26**, 5879–5886.
14 D. Zhang, L. Zhang, L. Shi, C. Fang, H. Li, R. Gao, L. Huang and J. Zhang, *Nanoscale*, 2013, **5**, 1127–1136.
15 G. Chen, F. Rosei and D. Ma, *Adv. Funct. Mater.*, 2012, **22**, 3914–3920.
16 H. X. Mai, L. D. Sun, Y. W. Zhang, R. Si, W. Feng, H. P. Zhang, H. C. Liu and C. H. Yan, *J. Phys. Chem. B*, 2006, **109**, 24380–24385.
17 H. Li, G. Qi, Tana, X. Zhang, W. Li and W. Shen, *Catal. Sci. Technol.*, 2011, **1**, 1677–1682.
18 K. Zhou, W. Xun, X. Sun, Q. Peng and Y. Li, *J. Catal.*, 2005, **229**, 206–212.
19 H. Wu and L. Wang, *Catal. Commun.*, 2011, **12**, 1374–1379.
20 Q. Dai, X. Wang and G. Lu, *Catal. Commun.*, 2007, **8**, 1645–1649.
21 H. Chang, J. Li, X. Chen, L. Ma, S. Yang, J. W. Schwank and J. Hao, *Catal. Commun.*, 2012, **27**, 54–57.

22 X. Wang, Y. Zheng and J. Lin, *Catal. Commun.*, 2013, **37**, 96–99.
23 W. Tang, W. U. Xiaofeng, G. Liu, L. I. Shuangde, L. I. Dongyan, L. I. Wenhui and Y. Chen, *J. Rare Earths*, 2015, **33**, 62–69.
24 P. Sudarsanam, B. Hillary, M. H. Amin, S. B. A. Hamid and S. K. Bhargava, *Appl. Catal., B*, 2016, **185**, 213–224.
25 J. Chen, N. Zhou, H. Wang, Z. Peng, H. Li, Y. Tang and K. Liu, *Chem. Commun.*, 2015, **51**, 10123–10126.
26 W. Zhan, X. Zhang, Y. Guo, L. Wang, Y. Guo and G. Lu, *J. Rare Earths*, 2014, **32**, 146–152.
27 P. Zhao, C. Wang, F. He and S. Liu, *RSC Adv.*, 2014, **4**, 45665–45672.
28 M. Cui, Y. Li, X. Wang, J. Wang and M. Shen, *J. Rare Earths*, 2013, **31**, 572–576.
29 F. Kleitz, S. H. Choi and R. Ryoo, *Chem. Commun.*, 2003, **9**, 2136–2137.
30 Q. Dai, X. Wang and G. Lu, *Appl. Catal., B*, 2008, **81**, 192–202.
31 F. He, J. Luo and S. Liu, *Chem. Eng. J.*, 2016, **294**, 362–370.
32 P. Ji, J. Zhang, C. Feng and M. Anpo, *J. Phys. Chem. C*, 2014, **112**, 17809–17813.
33 F. Jiao, A. Harrison, J. C. Jumas, A. V. Chadwick, W. Kockelmann and P. G. Bruce, *J. Am. Chem. Soc.*, 2006, **128**, 5468–5474.
34 Z. Wen, Y. Zhang, C. Dai and Z. Sun, *J. Hazard. Mater.*, 2015, **287**, 225.
35 Z. Wen, Y. Zhang, C. Dai, B. Chen, S. Guo, H. Yu and D. Wu, *Microporous Mesoporous Mater.*, 2014, **200**, 235–244.
36 P. Concepción, A. Corma, J. Silvestre-Albero, V. Franco and J. Y. Chane-Ching, *J. Am. Chem. Soc.*, 2004, **126**, 5523–5532.
37 M. Abecassis-Wolfovich, M. V. Landau, A. Brenner and M. Herskowitz, *J. Catal.*, 2007, **247**, 201–213.
38 Y. Dai, X. Wang, Q. Dai and D. Li, *Appl. Catal., B*, 2012, **111**, 141–149.
39 F. He, Y. Chen, P. Zhao and S. Liu, *J. Nanopart. Res.*, 2016, **18**, 1–10.
40 X. Tang, Y. Li, X. Huang, Y. Xu, H. Zhu, J. Wang and W. Shen, *Appl. Catal., B*, 2006, **62**, 265–273.
41 Y. Liao, M. Fu, L. Chen, J. Wu, B. Huang and D. Ye, *Catal. Today*, 2013, **216**, 220–228.
42 Z. Wang, G. Shen, J. Li, H. Liu, Q. Wang and Y. Chen, *Appl. Catal., B*, 2013, **138–139**, 253–259.
43 H. C. Yao and Y. F. Y. Yao, *J. Catal.*, 1984, **86**, 254–265.
44 Y. Dai, X. Wang, D. Li and Q. Dai, *J. Hazard. Mater.*, 2011, **188**, 132–139.
45 F. Arena, G. Trunfio, J. Negro, B. Fazio and L. Spadaro, *ChemInform*, 2007, **19**, 2269–2276.
46 H. Chang, J. Li, J. Yuan, L. Chen, Y. Dai, H. Arandiyan, J. Xu and J. Hao, *Catal. Today*, 2013, **201**, 139–144.
47 R. W. V. D. Brink, R. Louw and P. Mulder, *Appl. Catal., B*, 2000, **25**, 229–237.
48 Q. Dai, X. Wang and G. Lu, *Appl. Catal., B*, 2008, **81**, 192–202.
49 R. W. V. D. Brink, R. Louw and P. Mulder, *Appl. Catal., B*, 1998, **16**, 219–226.
50 Y. Peng, S. Yang, Z. Shi, Z. Meng and R. Zhou, *Appl. Catal., B*, 2015, **162**, 227–235.
51 X. Wang, Q. Kang and D. Li, *Catal. Commun.*, 2009, **86**, 166–175.